Article

Journal of the Brazilian Chemical Society

https://dx.doi.org/10.21577/0103-5053.20240097

J. Braz. Chem. Soc. **2024**, *35*, 11, e-20240097, 1-8

An Innovative Green Eco-Friendly Method for the Synthesis of Zinc Oxide (ZnO) Nanoparticles Using *Plinia cauliflora* Extract

Raissa C. Serejo,[a] Heloísa P. Macedo,[b] Rodolfo L. B. A. Medeiros,[a,b] Dulce M. A. Melo,[b,c] Gilvan P. Figueredo,*[,a] Marcelo M. Oliveira[a] and José H. G. Rangel[a]

[a]*Programa de Pós-Graduação em Química, Instituto Federal de Educação, Ciência e Tecnologia do Maranhão, Campus Monte Castelo, 65030-005 São Luís-MA, Brazil*

[b]*Programa de Pós-Graduação em Ciência e Engenharia de Materiais, Universidade Federal do Rio Grande do Norte, 59078-970 Natal-RN, Brazil*

[c]*Programa de Pós-Graduação em Química, Universidade Federal do Rio Grande do Norte, 59078-970 Natal-RN, Brazil*

ZnO nanoparticles were synthesized for the first time, using extracts from the leaf and peel of *Plinia cauliflora* (jabuticaba) fruit by varying the pH level of the reaction medium. The powders were obtained after calcination at 400 ºC and characterized by thermogravimetry (TGA), X-ray diffraction (XRD), Fourier transform infrared spectrophotometry (FTIR) and scanning electron microscopy (SEM). The results indicate that the use of jabuticaba leaf extract favored the stabilization of nanoparticles, providing smaller crystallite sizes and lower crystallinity. Crystallite sizes smaller than 50 nm were obtained using the leaf extract with pH level adjusted to 7 and 10. The morphology was strongly affected by both the extracts and the pH levels of the medium, and showed a flower-like shape when using jabuticaba peel extract at pH 7. Thus, the use of *Plinia cauliflora* extract showed a promising potential for the production of ZnO nanoparticles with different morphologies.

Keywords: zinc oxide, jabuticaba, green synthesis, nanopowder, morphology

Introduction

In today's world, nanotechnology is a highly prominent field in the development of advanced materials, involving the synthesis, design, manipulation and control of nanoscale materials, often between 1 and 100 nm, or whose physicochemical properties are superior to those of traditional materials.[1-4] Nanostructured oxides have been applied extensively in several areas of nanotechnology, including biomedicine,[5,6] semiconductors,[7] catalysis,[8,9] luminescent devices,[10] sensors,[11] solar cells[12] and photodetectors.[13]

Zinc oxide nanoparticles (ZnONPs) are part of a group of widely investigated semiconductor oxides such as SnO_2, TiO_2 and CuO. ZnONPs, in particular, stand out for their wide energy band and for being n-type semiconducting material suitable for photocatalytic, photovoltaic and photodetection applications.[14-16] In addition to their semiconductor activity, ZnONPs have also been explored for other applications, such as biomedical, due to their excellent antibacterial, antifungal, and anti-inflammatory properties, and low cytotoxic effects.[17] In a recent study, Marques *et al*.,[18] observed a selective inhibitory activity of multidrug-resistant bacteria by ZnONPs.

ZnONPs can be produced by a variety of techniques, including sol-gel,[10] precipitation,[19,20] hydrothermal,[8] microwave-assisted hydrothermal,[18] combustion reactions,[21] etc.[22] In response to environmental concerns, many studies[23-25] have focused on the search for partial or total substitution of toxic reagents for natural substances obtained from plant extracts. In this context, green synthesis has proved to be advantageous from the economic, operational and environmental points of view, and can contribute to the creation of methods that provide energy savings, reproducibility and lower costs.[24] Green methods are ecologically friendly because they are non-toxic, involve the use of harmless precursors,

*e-mail: gilvanfigueredo@ifma.edu.br
Editor handled this article: Célia M. Ronconi (Associate)

and do not require hazardous conditions such as high temperatures and pressures, nor toxic solvents.[26-28] In terms of structural quality, several advantages can be listed, such as the production of nanomaterials with uniform particle size, high purity and crystallinity, and the possibility of morphological alterations.[5,6] In the reaction medium, the organic biomolecules in extracts can act as complexing, polymerizing, reducing, precipitating and stabilizing agents of the inorganic precursor species of nanoparticles.[26] These characteristics have led several research groups to migrate from conventional routes to the green route.

Zinc oxide nanoparticles have been synthesized using several types of extracts, such as those obtained from the leaf of *Plectranthus amboinicus*,[29] *Ocimum basilicum*,[30] *Aloe barbadensis*,[31] *Cassia fistula*,[32] and *Solanum nigrum*.[33] However, *Plinia cauliflora* (jabuticaba) leaf and peel extracts have not yet been studied to obtain ZnO. Leaf and fruit extracts of *P. cauliflora* (jabuticaba) have been used in the green synthesis of silver nanoparticles.[34,35] Their composition is rich in pigments such as polyphenols, including flavonoids, tannic acid, and ellagitannin.[36] According to Bandeira *et al.*,[26] these compounds are better known as antioxidants and are responsible for the green synthesis of zinc oxide nanoparticles due to their ability to chelate zinc ions and act as stabilizers of the produced nanoparticles. These compounds participate in the mechanism of formation that occurs during synthesis. The role of biomolecules and pH of the solution in the final properties of ZnONPs has yet to be clarified, which makes this a pioneering study. In addition, jabuticaba fruits and peel exhibit antioxidant, anti-inflammatory, antimicrobial, antiproliferative activities, antitumor and neuroprotective effects, and are used in the treatment of diarrhea, asthma, chronic inflammation of the tonsils.[36,37]

Experimental

Obtainment of jabuticaba extracts and green synthesis of ZnO

Zinc oxides were synthesized by the green method, using *Plinia cauliflora* (jabuticaba) peel and leaf extracts and $Zn(NO_3)_2.6H_2O$ as precursors. Jabuticaba fruits and leaf were collected in the city of Natal, located in the state of Rio Grande do Norte, Brazil, at the following coordinates: latitude: –5.81029; longitude –35.20165. In the first step of the synthesis, the extracts were prepared using 20 g of green biomass in 100 mL of water under stirring and heating at 60 ºC for 1 h. The pH of the extracts was then measured, revealing a pH level of 3 for the peel extract and 5 for the leaf extract. Figure 1 shows a schematic representation of the collected biomass and prepared extracts.

Figure 1. Jabuticaba peel (a) and leaf (b) and their respective extracts.

The ZnO powders were synthesized by modifying the pH level of the two extracts, and without extract (standard). The synthesis of the standard ZnO was performed in a 600 mL beaker containing 70 mL of distilled water, to which were added 3 g of zinc nitrate (98%, Vetec, São Paulo, Brazil), resulting in a solution with pH 3. Two additional solutions with zinc nitrate were prepared, to which concentrated NH_4OH (ca. 30%, Vetec, São Paulo, Brazil), was added until one reached a pH level of 7 and the other one a pH of 10. The solution with pH 7 precipitated zinc oxide, while the solution with pH 10 was heated to 70 °C and held at this temperature for 30 min, after which precipitation occurred. In the syntheses using jabuticaba peel and leaf extracts, 30 mL of the extract were added to 20 mL of distilled water in a beaker, which was placed in an oven at 40 ºC for 30 min. Then, 3 g of zinc nitrate were added and the solution was stirred and heated continually until the solvent evaporated and a viscous suspension was obtained. The pH of the solution was measured, revealing a pH level of 3. In order to adjust the pH level to 7 and 10, NH_4OH was added to the medium to favor the development of hydrolysis, condensation or precipitation reactions within the system.[24] To eliminate organic matter and form the crystalline structure, all the samples were calcined for three hours in two steps. Step (*i*) 250 ºC for 1 h, and step (*ii*) 400 ºC for 2 h. The resulting materials were identified as: ZnO obtained from jabuticaba leaf extract (JLE), ZnO obtained from jabuticaba peel extract (JPE) and standard zinc oxide.

Characterization of ZnO

A thermogravimetric analysis (TGA) was conducted on a TGA 500 thermobalance (TA Instruments, New Castle, USA) to evaluate the decomposition of organic matter from the extract and the formation of ZnO phase. To this end, a 10 mg non-calcined sample was heated from room temperature to 800 ºC under a heating rate of 10 ºC min^{-1} and synthetic air flow of 60 mL min^{-1}, similar to the calcination environment.

The crystalline structure of the nanoparticles was examined by X-ray diffraction in a Shimadzu XRD-7000 diffractometer (Tokyo, Japan) operating at 30 kV and 30 mA, using Cu Kα radiation (λ = 1.5409 Å), angular scanning of 20-80º (2θ), scanning speed of 1º min^{-1} and step of 0.01º. The lattice parameters of the structure and the phases were analyzed using Rietveld refinement. The crystallite size was calculated using the Scherrer equation (equation 1),

$$T_c = \frac{0.89\lambda}{\beta\cos\theta} \quad (1)$$

where T_c is the crystallite size, λ is the wavelength (Cu Kα), β is the full width at half maximum (FWHM), and θ is the diffraction angle.

The morphology of the nanoparticles was evaluated under a field emission gun-scanning electron microscope (SEM-FEG, Zeiss Auriga 40, Germany). The samples were coated with a thin gold layer of approximately 70 nm.

The pure extract and the ZnO nanoparticles were analyzed by infrared absorption spectroscopy to check for the presence of organic groups after synthesis. The absorption band corresponding to biomolecules appears only in the spectrum of extracts and should disappear in the spectrum of nanoparticles. A Shimadzu IRPrestige-21 Fourier transform infrared (FTIR) spectrophotometer was used to analyze the samples, which were first pelletized by mixing them with a small amount of potassium bromide. The spectra were recorded in the region of 4000 to 400 cm^{-1}.

Results and Discussion

The TGA, Figure 2, conducted on non-calcined zinc oxides derived from jabuticaba leaf extract (JLE), peel extract (JPE), and standard zinc oxide reveals insightful information about the thermal behavior and decomposition of these materials. Overall, the results depict two distinct stages in the TGA process. The initial mass loss is attributed to the evaporation of water content within the samples, followed by subsequent losses associated with the decomposition of organic compounds, eventually forming ZnO. Notably, mass losses are found to be more significantly influenced by the pH level of the medium rather than the type of extract used.

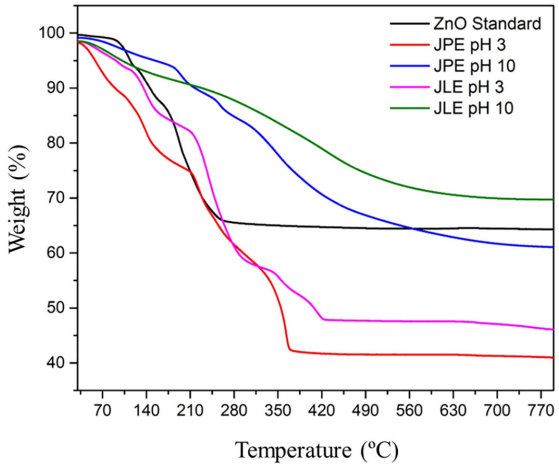

Figure 2. TGA curves of the synthesized ZnO. Standard sample synthesized at pH 3.

Samples prepared at a basic pH level exhibit minimal mass loss during precalcination, suggesting a significant reduction in mass, possibly due to a combustion reaction facilitated by biomolecules and ammonium hydroxide. Conversely, samples prepared in an acid medium display greater mass loss, indicating the formation of an organic-inorganic precursor without combustion during precalcination. Moreover, the thermal behavior of samples is influenced by the pH of the medium, revealing that the samples prepared at pH 10 generally exhibit lower mass loss compared to those synthesized at pH 3. This suggests that alkaline conditions may influence decomposition pathways, potentially resulting in more efficient removal of organic components during precalcination.

The final decomposition temperatures vary among samples, with those prepared using peel extract generally exhibiting lower final decomposition temperatures than those prepared with leaf extract, irrespective of the pH of the medium. This variation indicated differences in the composition of the extracts and their thermal stability.

These findings highlight the complex relationship between type of extract, pH levels, and thermal behavior of synthesized ZnO materials. Understanding these dynamics is essential to optimize synthesis conditions and tailor the properties of ZnO nanoparticles for various applications.

Figure 3 shows the X-ray diffractograms of the synthesized materials. All the materials show characteristic diffraction peaks corresponding to the (100), (002), (101), (102), (110), (103), (200), (112) and (201) crystallographic planes of zinc oxide with hexagonal wurtzite structure and

P63mc symmetry (JCPDS No. 01-089-0510). According to the diffractograms, all the materials are single-phase ZnO, revealing the efficiency of the green synthesis method to obtain pure zinc oxide. Moreover, the XRD patterns clearly indicate that the same pure crystalline structure can be obtained from both extracts (peel and leaf) and at different pH levels (3, 7 and 10).

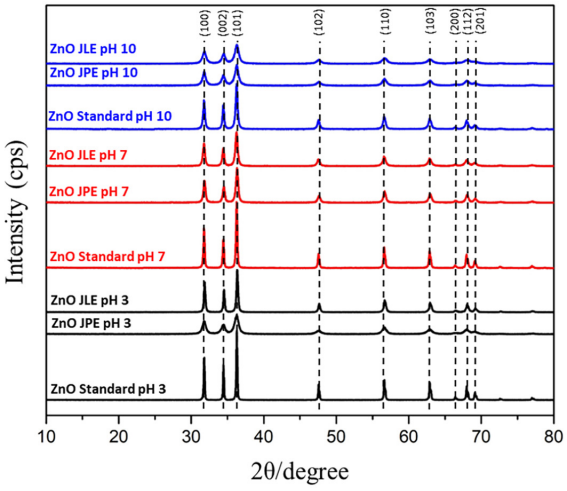

Figure 3. XRD patterns of synthesized ZnO.

Figures 4a and 4b illustrate the relationship between crystallinity and crystallite size according to the pH level of the synthesis medium using the two prepared extracts. The addition of extracts led to the formation of smaller crystallites and materials with lower crystallinity. In general, all the samples exhibited smaller crystallite sizes and lower crystallinity under basic conditions. Powders synthesized without extract (ZnO standard) and with leaf extract displayed larger crystallite sizes at acidic pH levels, demonstrating a significant reduction (80%) as the pH shifted towards basic level. In contrast, powders prepared with peel extract exhibited a distinct behavior, with smaller crystallite sizes and lower crystallinity in both acidic and basic conditions than in neutral medium. The powder synthesized from leaf extract in basic medium (ZnO JLE pH 10) exhibited the smallest crystallite size (15.7 nm) and the lowest degree of crystallinity (40.7%). On the other hand, the powder synthesized without extract in acid medium presented a larger crystallite size (238.9 nm) and high crystallinity (91.93%). Therefore, it can be inferred that an acidic medium favors higher crystallization than a basic medium, and that the presence of biomolecules from the extract stabilizes ZnO particle growth during the green synthesis process. The ZnO JLE pH 10 sample exhibited a smaller average crystallite size than the sizes commonly reported in the literature using methods such as sol-gel and precipitation,[14-20] microwave-assisted hydrothermal synthesis,[18] and green synthesis with *Nilgiriantus ciliantus*,[5] *Azadirachta indica* (Neem),[6] among other plant extracts.[26,27] Our results confirm the findings reported by Singh *et al.*,[38] and Nagarajan and Kuppusamy,[39] indicating that the increase in pH led to a decrease in particle size and agglomeration.

In order to understand the effect of the pH level and of jabuticaba extract on ZnO nanoparticle formation, it is valuable to identify the functional groups in the precalcined powders. Such investigation is performed via infrared spectroscopy analysis, which reveals the vibrations of the functional groups relating to the stretching of hydroxyls and carbon-oxygen bonds. Figures 5a and 5b present the FTIR spectra of the extracts and ZnO samples obtained at different pH levels. Bands (1) and (4), located at around 3500 and 1700 cm^{-1}, respectively, represent the vibrational modes of the O–H–O bonds. The band at 3500 cm^{-1} corresponds to symmetric bond stretching and is associated with the absorption of water molecules on the surface of the sample, while the band at 1700 cm^{-1} is related to asymmetric bond stretching. On the other hand, bands (2) and (3), which appear in the range of 2400 and 1300 cm^{-1}, respectively, indicate the existence of organic species in the material. The

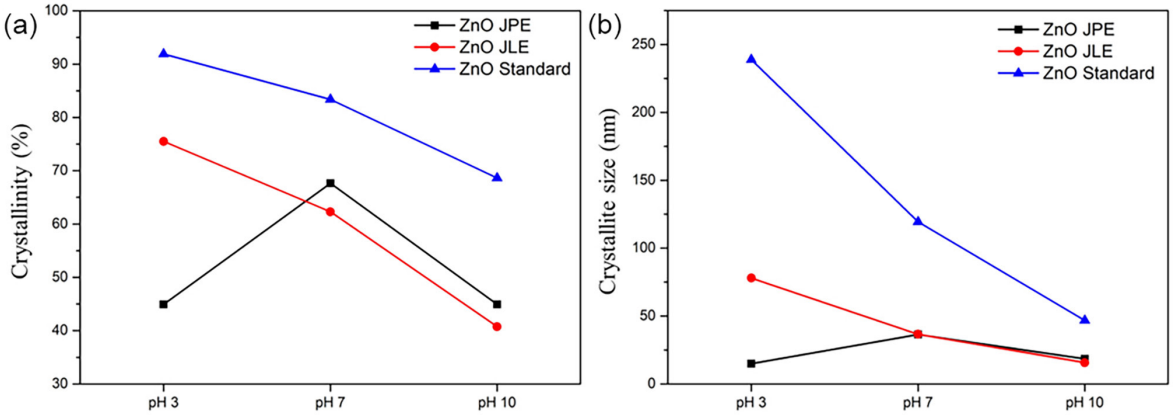

Figure 4. Correlation between crystallinity and crystallite size as a function of the pH level of synthesized ZnO.

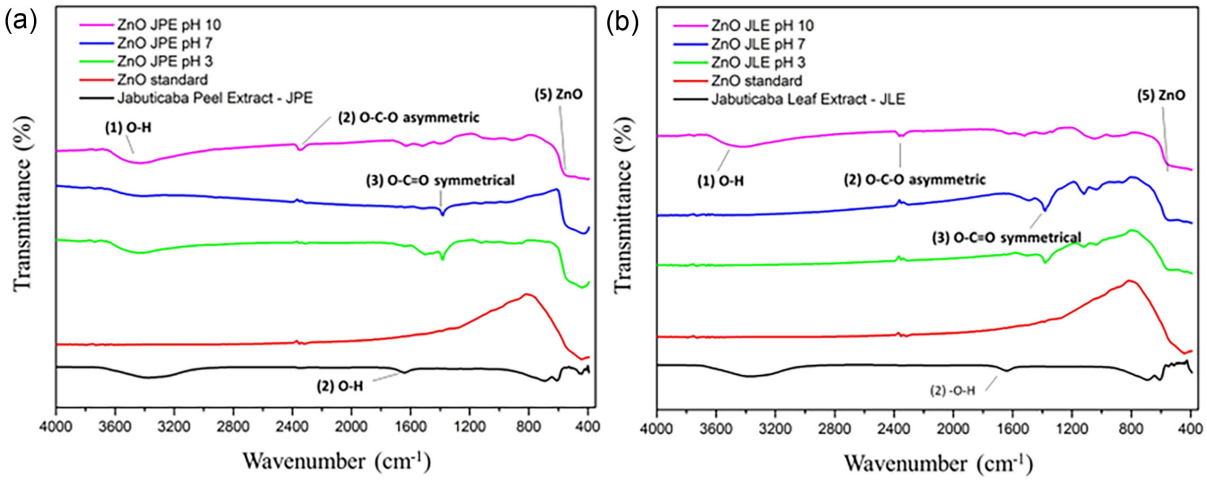

Figure 5. FTIR (KBr) spectra of the synthesized ZnO.

band (5) within the range of 500 cm^{-1} pertains to vibrational transitions of the Zn–O bond, evidencing its formation. A comparison with standard precalcined ZnO reveals the presence of functional groups derived from the extract.

The micrographs shown in Figure 6 reveal different ZnO morphologies, which are strongly dependent on the pH level of the medium during synthesis, indicating that the pH level of jabuticaba extract is essential to model the particle shape. The two extracts (peel and leaf) produced completely different morphologies compared to the standard ZnO. The use of ammonium hydroxide led to the modification of the particle morphology, since the number of OH^- groups

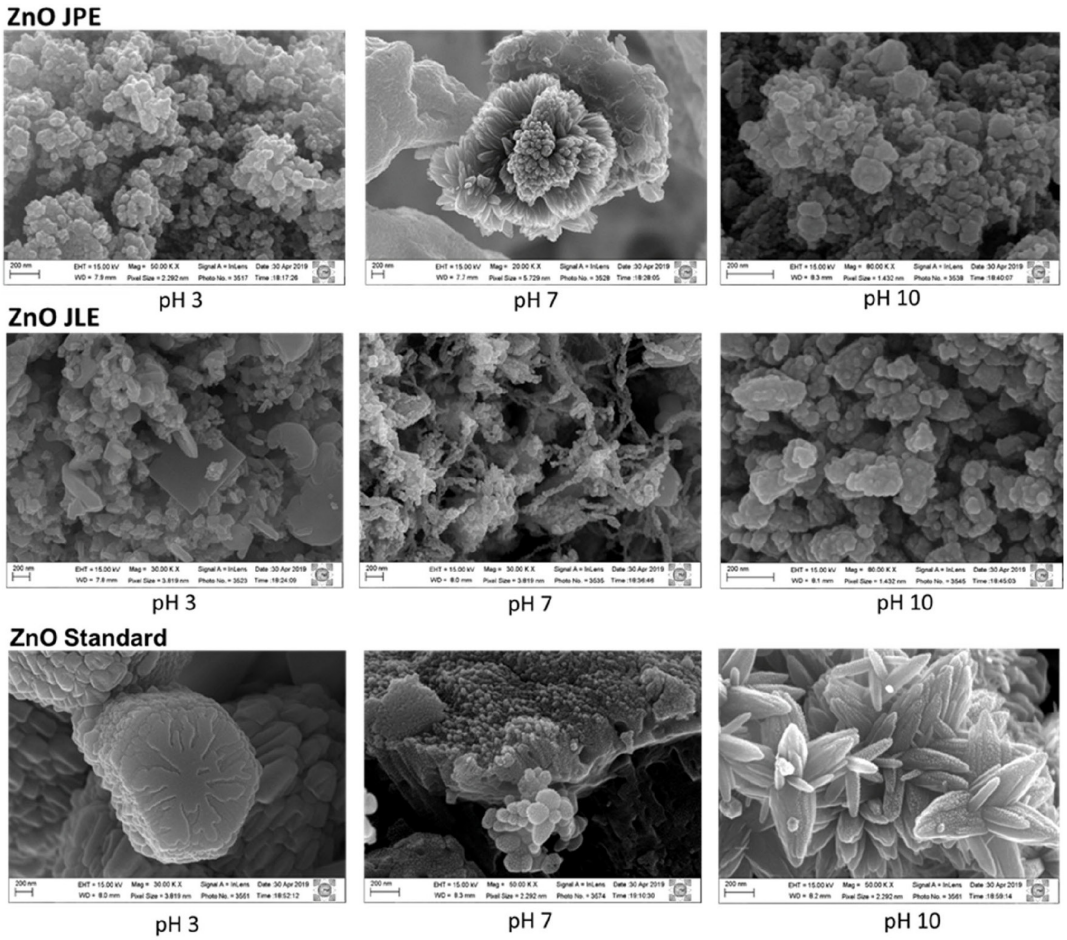

Figure 6. SEM micrographs of synthesized ZnO.

with Zn^{2+} affects the concentration of the intermediate compounds $Zn(OH)_2$ and $[Zn(OH)_4]^{2-}$. Pandit and Badnore[40] state that the morphology can change from ZnO nanoplates to nanospheres according to the concentration of these compounds. This behavior was observed in the ZnO synthesized with jabuticaba leaf extract (ZnO JLE), but only at pH 3 and pH 10 in that synthesized with peel extract (ZnO JPE). According to Patil *et al*.,[16] the formation of flower-shaped particles occurs through the reaction and nucleation of Zn^{2+} with hydroxyl groups to form $Zn(OH)_2$ precipitates. However, complex ions are usually unstable in a heating atmosphere, so $Zn(OH)_2$ decomposes into:

$$Zn(OH)_{2(ppt)} \rightarrow ZnO_{(s)} + H_2O_{(v)} \quad (2)$$

The zinc complex ion has a polarizing effect that can facilitate growth orientation along the [001] direction, resulting in an elongated rod-like or clustered morphology. $Zn(OH)_2$ decomposition leads to single ZnO molecules that act as growth units and are called seeds in crystal growth. Thus, the flower-like structure begins to grow in different directions starting from a small seed in the solution.[15,16] Therefore, the effect of the pH level during synthesis significantly altered the dynamics of zinc complex ion formation, resulting in different morphologies, as depicted in Figure 6.

A simplified mechanism of the green synthesis of ZnO nanoparticles using phytochemicals is proposed as follows: $[Zn^{2+}]$ (precursor solution) + phytochemicals (present in *Plinia cauliflora* extracts) → ZnONPs + secondary product(s). In this reaction, zinc ions (Zn^{2+}) present in the precursor solution react with the phytochemicals from *Plinia cauliflora* extracts. Phytochemicals act as chelating agents, forming intermediate products with zinc ions, leading to the formation of ZnO nanoparticles after the oxidation process. Phytochemicals can also act as capping and stabilizing agents, preventing the agglomeration of nanoparticles and ensuring their uniform dispersion. The end product of the reaction consists of ZnO nanoparticles, along with any side products that may be formed during the synthesis process.

Conclusions

The application of *Plinia cauliflora* peel and leaf extracts in green synthesis proved to be effective in the synthesis of ZnO nanoparticles. The use of jabuticaba leaf extract favored the production of smaller crystallite sizes and lower crystallinity. The decrease in crystallite size and crystallinity was attributed to the increase in pH levels, regardless of the use of the extract. Crystallite sizes below 50 nm were obtained using the leaf extract with pH levels adjusted to 7 and 10. The combination of extracts and different pH levels of the medium favored different ZnO morphologies. A flower-like morphology was developed using jabuticaba peel extract (ZnO JPE) at pH 7, while a plaque-like morphology was produced using leaf extract at pH 3.

The results obtained from TGA and subsequent characterization techniques provide valuable insights into the synthesis and properties of zinc oxide (ZnO) nanoparticles derived from jabuticaba extracts. The differences observed in mass loss and decomposition temperatures among samples prepared at different pH levels, using different types of extract, highlight the significant influence of synthesis conditions on the thermal behavior and composition of the resulting nanoparticles. Specifically, the TGA results suggest that the pH level of the medium plays a crucial role in determining the extent of organic decomposition and subsequent ZnO formation. These findings not only highlight the importance of careful control over synthesis parameters but also provide a fundamental understanding for the optimization of green synthesis routes for ZnO nanoparticles with tailored properties. Moreover, the comprehensive characterization using XRD, FTIR spectroscopy, and microscopic analysis elucidates the structural, chemical, and morphological characteristics of the synthesized ZnO nanoparticles. The consistent crystalline structure across all samples, regardless of type of extract and pH level, emphasizes the efficacy of the green synthesis method employed here. Furthermore, the variations observed in crystallite size, crystallinity, and morphology highlight the intricate interplay between synthesis parameters and the resulting nanoparticle properties. These insights not only advance our understanding of green synthesis approaches but also pave the way for the rational design and engineering of ZnO nanoparticles for diverse applications in fields such as catalysis, sensors, optoelectronics, and biomedical materials, alternatives promising avenues for future research and development efforts.

It is also important to emphasize, however, that further studies are required to delve deeper into the potential of these synthesized ZnO nanoparticles in specific applications such as photocatalysis, sensors, optoelectronic, and biomedical materials devices. Such additional research could provide a more comprehensive understanding of how the properties of these nanoparticles can be optimized to meet the specific demands of each application, thereby contributing to the development of more efficient and sustainable technologies.

Acknowledgments

This study was partly financed by the Coordenação de Aperfeiçoamento de Pessoal de Nível Superior-Brasil (CAPES) under Finance code 001 and CAPES Notice No. 13/2020 (Support Program for the Development of Postgraduate Studies in the Legal Amazon). The authors acknowledge IFMA for providing the infrastructure and financial support (National Scientific Research Exchange Program: IFMA Notice No. 146/2018). The authors also thank Fundação de Amparo à Pesquisa e Desenvolvimento Científico do Maranhão (FAPEMA) for its financial support, and the Central Analítica do Instituto de Química (UFRN), Departamento de Engenharia de Materiais (UFRN), and LABTAM/UFRN for its support in carrying out this work.

Author Contributions

Gilvan P. Figueredo supervised the research, writing and revision of the manuscript; Raissa C. Serejo was responsible for research, data analysis and writing of the manuscript; Heloísa P. Macedo collected the fruiting plant, and conducted research, and data analysis; Rodolfo L. B. A. Medeiros was responsible for research, data analysis and revision of the manuscript; Marcelo M. Oliveira, Dulce M. A. Melo and José H. G. Rangel undertook the overall supervision of this research and revision of the manuscript.

References

1. Sridevi, H.; Bhat, M. R.; Kumar, P. S.; Kumar, N. M.; Selvaraj, R.; *Appl. Nanosci.* **2023**, *13*, 5605. [Crossref]
2. Vinayagam, R.; Nagendran, V.; Goveas, L. C.; Narasimhan, M. K.; Varadavenkatesan, T.; Chandrasekar, N.; Selvaraj, R.; *Mater. Chem. Phys.* **2024**, *313*, 128787. [Crossref]
3. Kumar, R.; Kumar, M.; Luthra, G.; *Mater. Today: Proc. in press.* [Crossref]
4. Pansambal, S.; Oza, R.; Borgave, S.; Chauhan, A.; Bardapurkar, P.; Vyas, S.; Ghotekar, S.; *Appl. Nanosci.* **2023**, *13*, 6067. [Crossref]
5. Resmi, R.; Yoonus, J.; Beena, B.; *Mater. Today: Proc.* **2020**, *46*, 3062. [Crossref]
6. Iqbal, Y.; Malik, A. R.; Iqbal, T.; Aziz, M. H.; Ahmed, F.; Abolaban, F. A.; Ali, S. M.; Ullah, H.; *Mater. Lett.* **2021**, *305*, 130671. [Crossref]
7. Li, Y.; Huang, L.; Peng, J.; Wu, Y.; *Ceram. Int.* **2022**, *48*, 32436. [Crossref]
8. Catto, A. C.; Ferrer, M. M.; Lopes, O. F.; Mastelaro, V. R.; Andrés, J.; da Silva, L. F.; Longo, E.; Avansi Jr., W.; *Appl. Surf. Sci.* **2020**, *529*, 147057. [Crossref]
9. Bhole, R.; Gonsalves, D.; Murugesan, G.; Narasimhan, M. K.; Srinivasan, N. R.; Dave, N.; Varadavenkatesan, T.; Vinayagam, R.; Govarthanan, M.; Selvaraj, R.; *Appl. Nanosci.* **2023**, *13*, 6003. [Crossref]
10. Mo, Y.; Ye, D.; *Prog. Org. Coat.* **2022**, *167*, 106832. [Crossref]
11. Zhang, J.; Jia, X.; Liu, T.; Yang, J.; Wang, S.; Li, Y.; Shao, D.; Feng, L.; Song, H.; *Ceram. Int.* **2023**, *49*, 5861. [Crossref]
12. Salah, H. Y.; Abdelfatah, M.; El-Shaer, A.; Oraby, A. H.; *Ceram. Int.* **2023**, *49*, 7746. [Crossref]
13. Wang, J.; Chen, C.; Jin, M.; Zhu, Y.; Zhang, N.; *Opt. Mater.* **2023**, *135*, 113341. [Crossref]
14. Uribe-López, M. C.; Hidalgo-López, M. C.; López-González, R.; Frías-Márquez, D. M.; Núñez-Nogueira, G.; Hernández-Castillo, D.; Alvarez-Lemus, M. A.; *J. Photochem. Photobiol., A* **2021**, *404*, 112866. [Crossref]
15. Verma, R.; Pathak, S.; Srivastava, A. K.; Prawer, S.; Tomljenovic-Hanic, S.; *J. Alloys Compd.* **2021**, *876*, 160175. [Crossref]
16. Patil, V. L.; Vanalakar, S. A.; Vhanalakar, S. A.; Kamble, A. S.; Dongale, T. D.; Kurhe, D. N.; Kamble, P. P.; Patil, S. P.; Shendage, S. S.; Patil, P. S.; Kim, J. H.; *Zeitschrift fur Phys. Chemie* **2019**, *233*, 1183. [Crossref]
17. Vasile, B. S.; Oprea, O.; Voicu, G.; Ficai, A.; Andronescu, E.; Teodorescu, A.; Holban, A.; *Int. J. Pharm.* **2014**, *463*, 161. [Crossref]
18. Marques, G. N.; Moreira, A. J.; Nóbrega, E. T. D.; Braga, S.; Argentin, M. N.; Camargo, I. L. B. C.; Azevedo, E.; Pereira, E. C.; Bernardi, M. I. B.; Mascaro, L. H.; *J. Environ. Chem. Eng.* **2024**, *12*, 111870. [Crossref]
19. Mac, V. H.; Vu, A. T.; *J. Chinese Chem. Soc.* **2022**, *69*, 1997. [Crossref]
20. Gines-Palestino, R. S.; Montalvo-Romero, C.; Luna-Solano, G.; Amador-Gómez, L. P.; Cantú-Lozano, D.; *J. Braz. Chem. Soc.* **2024**, *35*, e-20230092. [Crossref]
21. Jinendra, U.; Bilehal, D.; Nagabhushana, B. M.; Kumar, A. P.; Afzal, M.; Shivamallu, C.; Majani, S. S.; Kollur, S. P.; *J. Mol. Struct.* **2024**, *1305*, 137701. [Crossref]
22. Criado, D.; Zúñiga, A.; Pepinelli, A.; *J. Braz. Chem. Soc.* **2024**, *35*, e-20230117. [Crossref]
23. Rocha, M. B. C.; de Araújo, T. R.; Medeiros, R. L. B. A.; Oliveira, M. M.; de Figueredo, G. P.; *Res. Soc. Dev.* **2021**, *10*, e399101623406. [Crossref]
24. Benitez-Salazar, M. I.; Niño-Castaño, V. E.; Dueñas-Cuellar, R. A.; Caldas-Arias, L.; Fernández, I.; Rodríguez-Páez, J. E.; *J. Environ. Chem. Eng.* **2021**, *9*, 106544. [Crossref]
25. Rai, R. S.; P, G. J.; Bajpai, V.; Khan, M. I.; Elboughdiri, N.; Shanableh, A.; Luque, R.; *Environ. Res.* **2023**, *221*, 114807. [Crossref]
26. Bandeira, M.; Giovanela, M.; Roesch-Ely, M.; Devine, D. M.; da Silva Crespo, J.; *Sustainable Chem. Pharm.* **2020**, *15*, 100223. [Crossref]
27. Agarwal, H.; Venkat Kumar, S.; Rajeshkumar, S.; *Resour. Technol.* **2017**, *3*, 406. [Crossref]

28. Borges, S. F.; Andrade, K. S.; Vaz, E. C.; Morais Neto, M. D.; Cabral, A. A.; Sobrinho, E. V.; da Rocha, C. Q.; de Figueredo, G. P.; *Quim. Nova* **2024**, *47*, e-20240034. [Crossref]
29. Roshni, A.; Thambidurai, S.; *Mater. Chem. Phys.* **2022**, *291*, 126739. [Crossref]
30. Malik, A. R.; Sharif, S.; Shaheen, F.; Khalid, M.; Iqbal, Y.; Faisal, A.; Aziz, M. H.; Atif, M.; Ahmad, S.; Fakhar-e-Alam, M.; Hossain, N.; Ahmad, H.; Botmart, T.; *J. Saudi Chem. Soc.* **2022**, *26*, 101438. [Crossref]
31. Naik, R.; Naveen Kumar, A.; Shanbhag, V.; Ravikumar, C. R.; Revathi, V.; Basavaraju, N.; Prashantha, S. C.; Girish, K. M.; Nagabhushana, H.; *Inorg. Chem. Commun.* **2022**, *143*, 109760. [Crossref]
32. Suresh, D.; Nethravathi, P. C.; Udayabhanu; Rajanaika, H.; Nagabhushana, H.; Sharma, S. C.; *Mater. Sci. Semicond. Process.* **2015**, *31*, 446. [Crossref]
33. Ramesh, M.; Anbuvannan, M.; Viruthagiri, G.; *Spectrochim. Acta, Part A* **2015**, *136*, 864. [Crossref]
34. Franzolin, M. R.; Courrol, D. S.; Silva, F. R. O.; Courrol, L. C.; *Molecules* **2022**, *27*, 6860. [Crossref]
35. de Oliveira Gonçalves, K.; Silva, F. R. O.; Courrol, L. C.; *Appl. Phys. A: Mater. Sci. Process.* **2022**, *128*, 692. [Crossref]
36. Mannino, G.; Perrone, A.; Campobenedetto, C.; Schittone, A.; Margherita Bertea, C.; Gentile, C.; *Food Chem.* **2020**, *307*, 125515. [Crossref]
37. Leite-Legatti, A. V.; Batista, A. G.; Dragano, N. R. V.; Marques, A. C.; Malta, L. G.; Riccio, M. F.; Eberlin, M. N.; Machado, A. R. T.; de Carvalho-Silva, L. B.; Ruiz, A. L. T. G.; de Carvalho, J. E.; Pastore, G. M.; Maróstica Jr., M. R.; *Food Res. Int.* **2012**, *49*, 596. [Crossref]
38. Singh, A. K.; Pal, P.; Gupta, V.; Yadav, T. P.; Gupta, V.; Singh, S. P.; *Mater. Chem. Phys.* **2018**, *203*, 40. [Crossref]
39. Nagarajan, S.; Arumugam Kuppusamy, K.; *J. Nanobiotechnol.* **2013**, *11*, 39. [Crossref]
40. Pandit, A. B.; Badnore, A. U.; *Chem. Eng. Process. Process Intensif.* **2017**, *122*, 235. [Crossref]

Submitted: February 3, 2024
Published online: June 6, 2024